Effects of oxygen on the Liquid Silicon Infiltration (LSI) process

Peter Josef Hofbauer [a],[*], Friedrich Raether [b]

[a] *ArianeGroup GmbH, 82024, Taufkirchen, Germany*
[b] *Fraunhofer Center for High Temperature Materials and Design HTL, 95448, Bayreuth, Germany*

ARTICLE INFO

ABSTRACT

The Liquid Silicon Infiltration (LSI) process has been in use for decades for the series production of components of various SiC materials as well as for environmental barrier coatings. However, high rejection rates and variations in quality still occur. One major cause of this are oxygen impurities in the furnace atmosphere during the infiltration. They can significantly disturb the siliconization process resulting in a discoloration of the component surfaces and an incomplete infiltration of the pore channels. Using different preforms, measuring methods and furnaces, the influence of oxygen on the LSI process was investigated systematically. It was demonstrated that the phenomenon is effective in general and also affects other processes such as sintering of non-oxide ceramics. The mechanisms that can disrupt or even prevent the infiltration and sintering processes have been identified. Methods for the continuous monitoring of the furnace atmosphere are compared. Measures are presented to reduce the oxygen concentration and subsequently quality degradation and rejection rates.

1. Introduction

Liquid Silicon Infiltration (LSI) is the most economical process for the production of components made of C_f/SiC or SiC_f/SiC, and the infiltration kinetics is well understood (Note that the index ‚f' indicates the respective material of the reinforcing fibers) [1,2]. Common applications of these materials are ceramic brake disks made of C_f/SiC or components for gas turbines made of SiC_f/SiC, as well as structural parts for high-quality optical systems made of SiC green parts, among many others [3–5]. The LSI process is also used for surface siliconization of components, for example to achieve gas tightness, or to protect components from corrosive fluids (environmental barrier coating, EBC) [6, 7]. It is performed in graphite furnaces at temperatures above the melting point of silicon (1413 °C) in inert gas atmosphere – usually at low pressure [8]. The silicon melt is soaked into the porous preforms by capillary forces. It partially reacts with carbon contained in the preform. The remaining silicon solidifies during cooling of the components and completely fills the pore channels.

Despite the long-lasting application of the LSI process in serial production, high rejection rates or variations in quality occasionally arise. Thus, in some instances components are not completely infiltrated, or coatings delaminate and peel off. This can be caused by oxygen impurities, which are always present to some extent in practice in the graphite furnaces. In this work, the following section illustrates the influence of oxygen on the siliconization using two examples at component level. The third section presents detailed investigations by structural analysis of reaction products and thermodynamic calculations. Based on these results, validation experiments were planned which are presented in the fourth section. In the fifth section, results are discussed and compared with other heating processes in graphite furnaces, e. g., sintering of non-oxide ceramics. Finally, appropriate measures for prevention of oxygen effects in graphite furnaces are outlined.

## 2. Phenomenological description of failed siliconizations

2.1. Example 1: Infiltration of liquid silicon into porous C_f/C preform

A preform was used made of short fiber reinforced carbon (C_f/C), as it is typical for the manufacture of ceramic brake disks. The most common way to produce these preforms is by warm pressing of carbon short fiber bundles (typical length 6 mm) with phenolic resin as a binder. After this, the preform is pyrolyzed by heating up to 1200 °C to obtain a porous (C_f/C) material that can be infiltrated by liquid silicon [3].

A part of such a preform was used for infiltration with liquid silicon at the Fraunhofer Center for High Temperature Materials and Design (HTL). The sample was mounted on three wicks through which the silicon enters the preform (see Fig. 1). The wicks were made from beech wood, which was pyrolyzed before use for siliconization [1]. The silicon
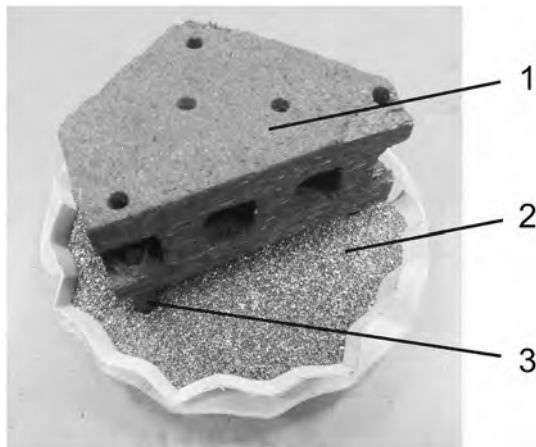
Fig. 1. Set-up for the liquid silicon infiltration. – 1: Preform (thickness: 40 mm, length: 110 mm, width: 80 mm), 2: Silicon granulate, 3: Porous wick made of pyrolized beech wood for capillary driven transport of melt silicon into the preform.

was provided as granulate with particle diameters between 0.2 and 0.8 mm (Silgrain HQ from Elkem) in a crucible made of graphite foil (SIGRAFLEX® 0.75 mm thickness). To avoid siliconization of the graphite foil, it was coated with boron nitrite (BN).

The infiltration set-up was mounted in the furnace chamber of a special measuring furnace called TOM_ac (Fig. 2). TOM_ac had been developed to study high-temperature processes in situ. The cylindrical furnace chamber was equipped with two opposing windows, located at the same height, with their optical axis cutting the vertical axis of the furnace [9,10]. The sample was aligned to the optical axis to enable recording of the infiltration with a CMOS camera. As with all other furnaces used in the present study, the resistance heaters were made of graphite, the furnace insulation was made of graphite felt and the furnace was encapsulated in a vacuum tight water-cooled steel chamber.

In order to investigate the influence of oxygen on the infiltration behavior, the furnace was opened and exposed to ambient air with the sample inside for 72 h. This allowed species such as water vapor, hydro carbons and CO_2 to be adsorbed at all surfaces: especially in the graphite felt insulation of the furnace, as well as in the wicks, preform and the silicon granulate. The furnace was closed, evacuated to 0.5 mbar and flooded with argon at ambient pressure. Argon flow gas purity was better than 99.999% in all experiments reported in the present paper. The heating cycle was performed in stationary argon atmosphere. The set-up was heated from room temperature to 1350 °C at 10 K/min. After
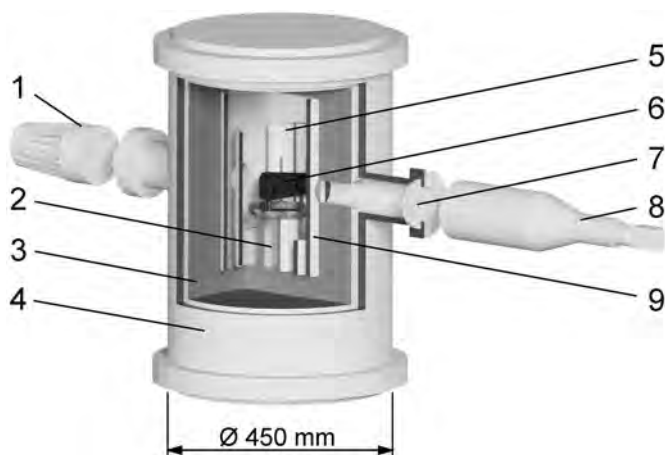
a holding time of 30 min, it was heated at 2 K/min to 1420 °C and after a further holding time of 30 min–1680 °C at 4 K/min. The furnace was then kept for 75 min at the maximum temperature of 1680 °C before being cooled to 1480 °C at 2 K/min and then to room temperature at 16 K/min. To monitor the oxygen concentration in the furnace, CO measurements were carried out. For this purpose, gas samples were extracted during heating up at 1000 °C as well as at 1420 °C using a rotary vane pump. The CO concentration was determined in the exhaust gas line using an electrochemical combustion gas analyzer (IM 1400 from IM Environmental Equipment). During the heating cycle, the formation of whiskers on the bottom side of the preform was observed. These formed above 1400 °C and were already clearly visible after a holding time of 30 min at 1420 °C (see Fig. 3).
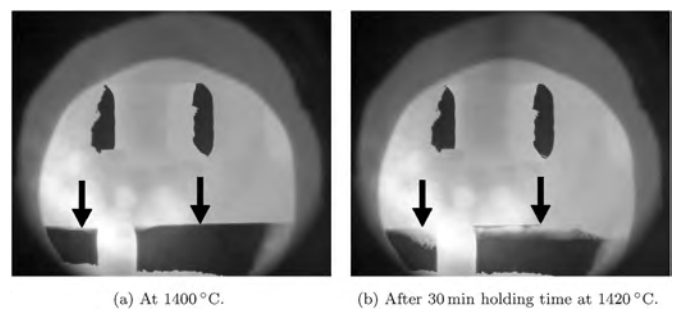
After cooling, it was observed that whiskers had also formed on the wicks, especially at the section of the wick that was dipped in the silicon melt (Fig. 4). The silicon granules around the wicks formed a layer, which did not melt and maintained their original shape. Apparently, a passivation layer was formed which had prevented the infiltration of the wicks with molten silicon. The preform was still porous after the heating cycle.

2.2. Example 2: Reaction bonded environmental barrier coating

For dual-mode ramjets in future hypersonic vehicles, ArianeGroup develops near net shape fiber preforms with integrated cooling channels via a combination of braiding and stitching technologies. To densify the textile preforms made out of pyrolytic carbon coated carbon fibers, a chemical vapor infiltration process is applied, producing a C_f/C-material with low porosity called CARBOTEX®. For the application as a combustion chamber, the surface of the hot gas wall is coated with a silicon containing slurry to produce a reacted, bonded, airtight Si/SiC layer by the LSI-process [11]. Fig. 5 shows a slurry-coated sample cut out of a preform for a combustion chamber.

For surface siliconization, the CARBOTEX® sample was deposited in a graphite heated hood furnace (see Fig. 6). As with the previous example, the CO concentration in the furnace atmosphere was also measured during the LSI process. For this purpose, a laser photometer was mounted at the furnace, which essentially consists of a laser diode and a photo detector. The emitted laser light has a wavelength that is adsorbed by CO (2.300 nm). Thus, the intensity measured by the photo detector is proportional to the CO concentration in the furnace, and a CO profile can be created over time and temperature.

Similar to the liquid silicon infiltration of brake disks, surface siliconization as oxidation protection and redensification of CARBOTEX®-components has been a standardized process for decades at ArianeGroup. However, there are still failed surface siliconizations. They are characterized by the fact that the previously applied slurry layer does not penetrate into the surface region of the preform (Fig. 7). It remains on the surface as a brittle, greenish layer and can easily be scratched off. These components have to be cleaned, coated with slurry and heat-

Fig. 2. Schematic view of the measuring furnace TOM_ac with a test sample in the center of the furnace.

(a) At 1400 °C.   (b) After 30 min holding time at 1420 °C.

Fig. 3. Whisker formation on the bottom side of the preform during heat treatment in TOM_ac. – The images were made with an infrared camera. The arrows mark the bottom side of the preform where the whiskers have formed.
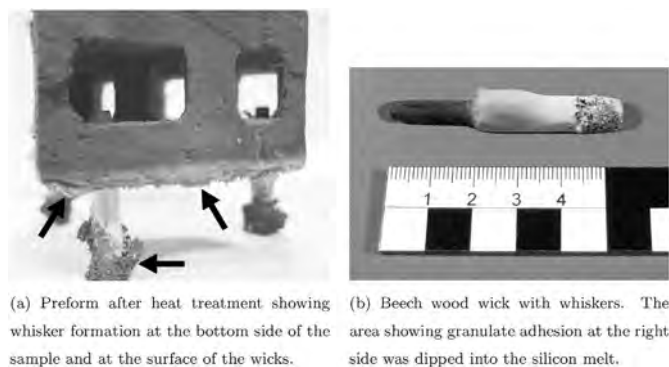
(a) Preform after heat treatment showing whisker formation at the bottom side of the sample and at the surface of the wicks.

(b) Beech wood wick with whiskers. The area showing granulate adhesion at the right side was dipped into the silicon melt.

Fig. 4. Preform after failed silicon infiltration and beech wood wick, respectively.

Fig. 5. Charged CARBOTEX® sample (thickness: 20 mm, length: 80 mm, width: 80 mm). – 1: environmental barrier coating made of silicon slurry, 2: CARBOTEX® substrate, 3: graphite bars as support auxiliaries.
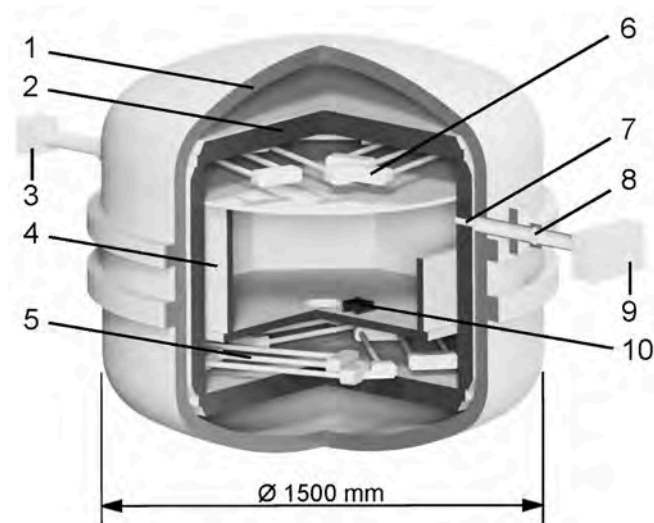

Fig. 6. Vacuum furnace (hood furnace) with measurement device.

treated again, until the surface siliconization has been successful.

3. Analysis of reaction products and thermodynamic calculations

3.1. Microstructure analysis

In order to determine the composition of the slurry layer (compare Fig. 7), which appears green and brittle after the failed heat treatment, both the coating and the silicon used were investigated. For this purpose, samples were extracted from the layer, which was not absorbed into the substrate, ground in an agate mill and examined by X-ray fluorescence analysis in helium atmosphere. In addition, a reference sample was investigated by grinding a successfully infiltrated EBC (compare Fig. 18 in section 4). Likewise, a sample of the greenish silicon granulate was examined after unsuccessful siliconization via wicks as shown in Fig. 4a. All samples were analyzed by X-ray diffractometry (PANAlytical), and the phase composition was estimated via the software High Score Plus. Results are summarized in Table 1.

The aluminum impurities identified by RFA (compare Table 1) led to an investigation of the used silicon powder (Silgrain® HQ MicronCut 0 … 10 μm with 99.8% purity from Elkem). Energy-dispersive X-ray spectroscopy (EDX) was used in a scanning electron microscope (SEM) to investigate the impurities on the surface of the silicon grains (Fig. 8). The EDX spectra indicate that the impurities include alumina (see marked spots in Fig. 8a and corresponding spectra in Fig. 8b). Other authors, such as Andersen et al., also detected aluminum with about 0.1% as the largest contamination on the silicon surface using X-ray fluorescence analysis (XRF) [12].

In addition, silicon powder samples were analyzed by EDX, which were heat-treated under vacuum at 1375 °C (see Fig. 9). Compared to the EDX spectra of untreated silicon powder, the spectra of the heat-treated silicon showed a fine-grained layer consisting of Si and C, which was attributed to SiC (see Fig. 9a). The same composition was identified for the whiskers, which had formed in the TOM_ac furnace (compare Fig. 4). SEM images of the white to beige fluffy coating on the carbon preform and the wick are shown in Fig. 9b. The SiC whisker on the carbon preform without direct contact to the silicon bulk clearly shows that SiC formation below the Si melting point is a gas phase reaction between gaseous SiO and CO, which is well described by Saito et al. [13]. Similarly, the gas phase reaction of CO with solid silicon for the formation of SiC whiskers was investigated specifically below the Si melting point in other works [14].

3.2. Thermodynamic analysis of the system Si–C–O

The elements, which are most relevant during siliconization, are: C, Si and O – the latter coming from impurities introduced by the charge and the furnace materials, by flushing gases or vacuum leaks. In a graphite furnace, oxygen reacts to CO_2 respectively CO according to the well-known Boudouard equilibrium:

$$2\,CO(g) \quad \longleftrightarrow \quad C(s) + CO_2(g). \tag{1}$$

At high temperatures, CO is the dominating gaseous species. The activity of carbon $a(C)$ is controlled by the partial pressures of CO and CO_2 in the furnace atmosphere according to reaction 1 [15]:

$$a(C) = \frac{p_{CO}^2}{p_{CO_2}} \cdot \exp\left(\frac{\Delta G^0}{RT}\right) \approx \frac{p_{CO}^2}{p_{CO_2}} \cdot \exp\left(\frac{20060}{T} - 20.57\right) \tag{2}$$

Where ΔG^0 is the standard free energy of formation, T is the absolute temperature in K, R is the gas constant and p_{CO} and p_{CO_2} are partial pressures specified in bar.

Just like [15], the effect of CO and C activity on the stability of the three solid phases in the system Si–O–C is illustrated using predominance diagrams. They show the regions of the most stable phase at
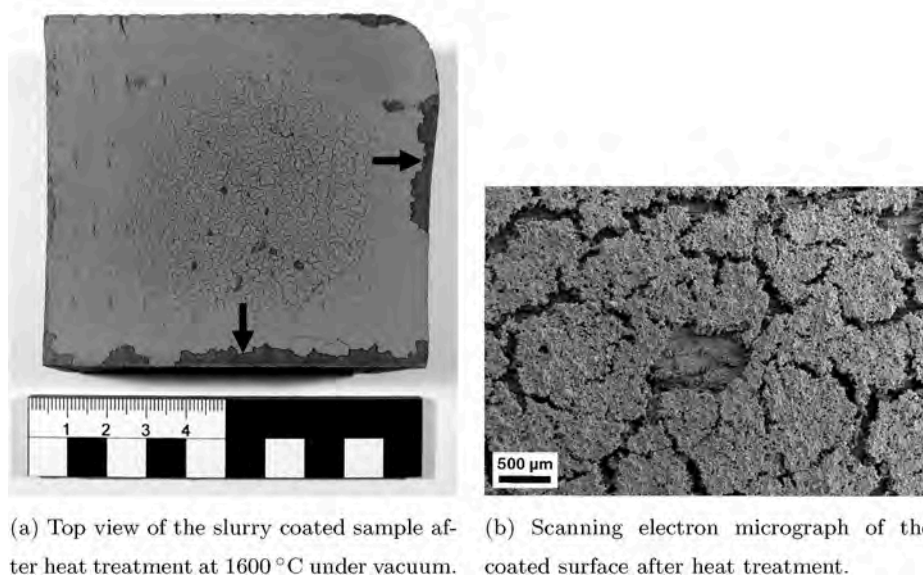
(a) Top view of the slurry coated sample after heat treatment at 1600 °C under vacuum.

(b) Scanning electron micrograph of the coated surface after heat treatment.

Fig. 7. Environmental barrier coating after failed surface infiltration.

Table 1
Results of X-ray diffractometry (XRD) and X-ray fluorescence analysis (XRF), analyses of samples from successful and unsuccessful EBC layers as well as Si granules from failed LSI experiment.

Sample	Coleration	XRD analysis	XRF analysis
successful EBC (see Fig. 18)	grayish to black	SiC: 96.7%	SiC: 97.6%, oxides: 2.4% with 1.2% Al_2O_3
failed EBC (see Fig. 7)	greenish	SiC: 100,0%	SiC: 99.5%, oxides: 0.5% with 0.1% Al_2O_3
Si granules after failed LSI (see Fig. 4a)	greenish to beige/white	SiC: 99.4%	SiC: 99.6%, oxides: 0.4% with 0.3% Al_2O_3

(a) SEM image of a silicon particle surface as used for the slurry. – The positions 1…3 have been marked with arrows where an EDX analysis has been performed.

(b) EDX analysis of the positions 1…3 marked in Figure 8a – At position 3, a significant Al peak is visible.

Fig. 8. SEM image of a silicon grain surface and corresponding EDX analysis of the surface and its impurities.

constant temperature (see Fig. 10). The diagrams were calculated using the program FACTSAGE (FACTSAGE version 6.3, GTT-Technologies, Herzogenrath, Germany). At high carbon activity, SiC and – at higher CO partial pressure – SiO_2 are stable. The transition from SiC to SiO_2 shifts to higher CO partial pressure with increasing temperature. At low carbon activity and low CO partial pressure, Si is stable as well and the Si area expands with increasing temperature. However, at 1400 °C, Si is only stable if the carbon activity is smaller than approximately 0.01 and CO partial pressure is beyond 100 ppm (compare Fig. 10).

To understand the evolution of phases in the actual process, a two-step approach for the thermodynamic calculations is helpful.

Considering the large amount of carbon contained in the graphite furnace, we first take into account the incoming Ar stream, which is contaminated by O_2. The equilibrium partial pressures of the two dominating gas species CO and CO_2 are calculated according to Equation (1). Fig. 11 shows the ratio of the partial pressures of CO_2 and CO at a carbon activity of 1, as it is expected in the graphite felt and close to the graphite heaters. As it is well known, the CO_2/CO-ratio decreases steeply with temperature. At temperatures above 800 °C, CO partial pressure equals the total pressure of the carbon species in the gas phase (comp. Fig. 11). It is twice as much as the oxygen partial pressure in the incoming gas stream. Ideal gas behavior can be assumed and equilibria depend on the partial pressures of the reactants and not on total pressure, which includes the flushing gas Ar.

In the second step, the interaction of CO with the sample is considered. The equilibria in the system Si – C – O – Ar have been calculated at different temperatures and CO partial pressures using Factsage (Fig. 12 a). Carbon activity was fixed at 1 and total pressure was 1 bar. Besides carbon, SiO_2 and SiC are the only stable solid phases: SiO_2 at low temperatures and SiC at high temperatures. It can be seen, that the transition from SiO_2 to SiC shifts to higher temperatures with increasing CO partial pressure (Fig. 12 b). The partial pressure of SiO, which is the dominating Si species in the gas phase, increases with temperature (Fig. 12 a). The slope drastically decreases at the transition from SiO_2 to SiC leading to a reversal in the relation of SiO partial pressure to CO partial pressure.

4. Evaluation experiments

4.1. Investigation of silicon powders

The formation of SiC on Si powder and granulate was systematically investigated in 12 heating runs which are summarized in Table 2. The first four experiments were performed in a laboratory furnace (diameter of usable volume 100 mm, height 150 mm) using a simple test setup. Approximately, 1.7 g of silicon powder (Silgrain HQ MicronCut 1 … 10 µm) was deposited on a graphite sheet (with 0.5 mm thickness from Sindlhauser Materials) which has previously been heated under vacuum at 1500 °C. The heat treatment is necessary to remove additives from the manufacturing process of the sheet [16]. Before heating three evacuation (to 10^{-2} mbar and flushing to normal pressure) cycles with argon were performed. Pressure during the heating cycle was approximately 10 mbar due to the pyrometer glass flushing with argon at 0.3 Nl/min.
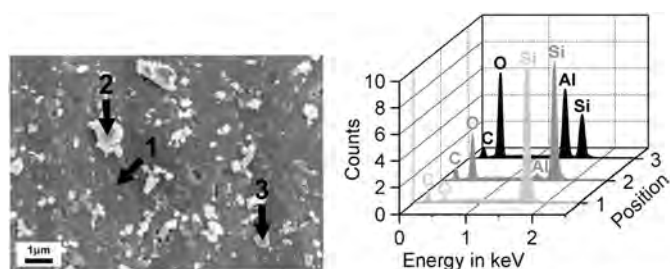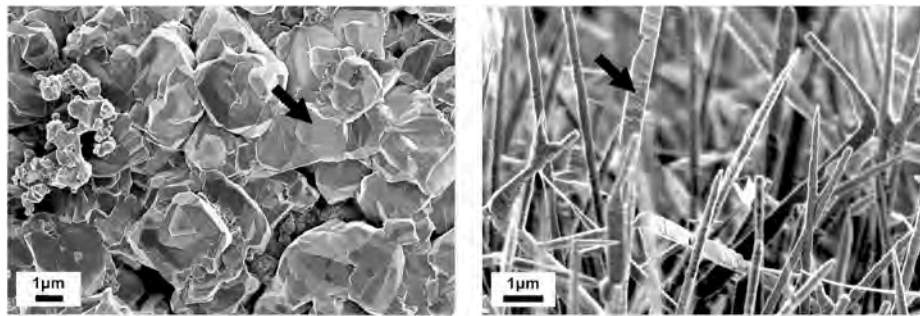
(a) SEM image of the silicon powder heat treaded at 25 mbar at 1375 °C. – EDX analysis indicates that the fine grained layer is SiC.

(b) SEM image of the whiskers formed on the wick (see Figure 4b). – EDX analysis confirmed that the whiskers are composed of Si and C.

Fig. 9. SEM images of the fine grained SiC layer formed by heat treatment of the silicon powder as well as whiskers formed on carbon substrates e. g. preforms or wicks.
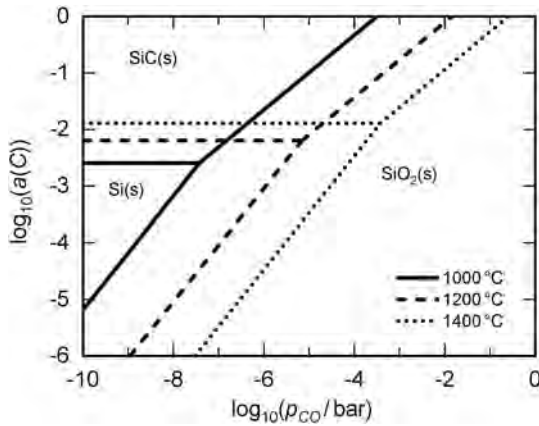

Fig. 10. Predominance diagrams in the system Si–O–C for three different temperatures indicating the regions of the most stable solid phases: Si, SiC and SiO_2 versus carbon activity $a(C)$ and CO partial pressure $p(CO)$.
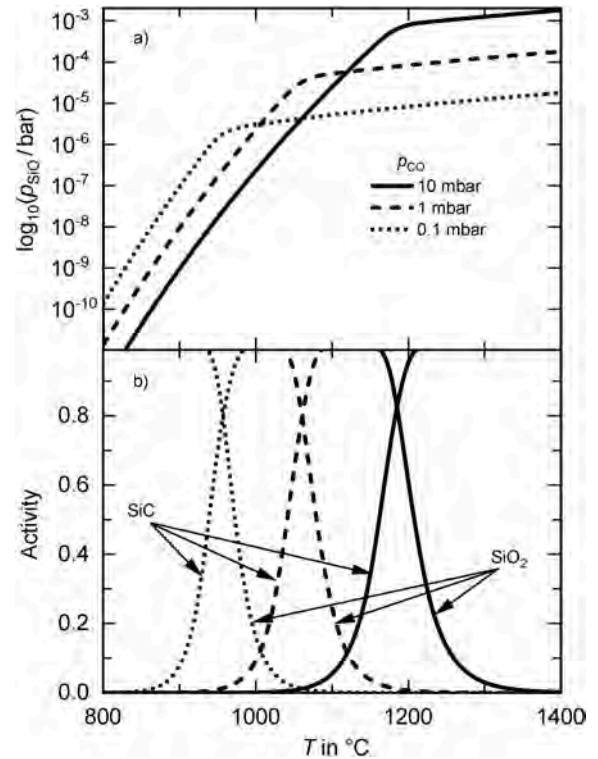

Fig. 11. Ratio of CO_2 and CO partial pressure (left y-axis) and molar fraction of CO (right y-axis) versus temperature at carbon activity of 1 and different pressures.

Fig. 12. Equilibrium data in the system Si – C – O – Ar at different partial pressures of CO, a total pressure of 1 bar and an activity of carbon of 1: a) partial pressure of SiO and b) activity of SiC and SiO_2 respectively.
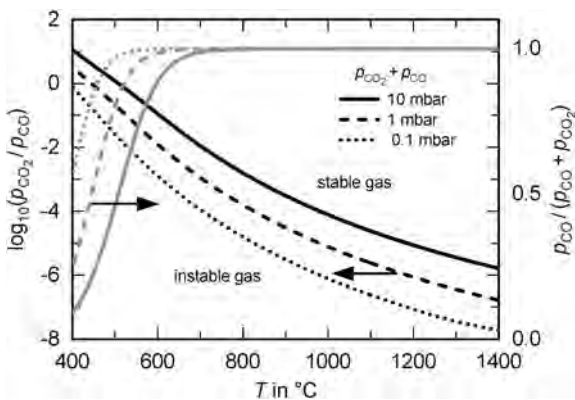
The heating rate was 10 K/min from room temperature to the target temperature, and after a holding time of 3 h the sample was cooled at 10 K/min to 1000 °C and then naturally cooled to room temperature. As an example, Fig. 13 shows a sample before and after the heating cycle. As described above, the SiC layer is easily recognizable by the gray to beige/greenish color.

Samples heat treated at different temperatures were photographed with the same illumination conditions. The images were converted into grayscale images, and the average gray value within a circular area with a diameter of approx. 15 mm in the center of the powder samples was determined using MATLAB. In order to exclude possible distortions, e. g. by boron nitrite powder, the brightest 3% of the gray values were excluded from averaging. The average gray values obtained are shown in Fig. 14 (curve 1). They rise at about 1200 °C indicating increasing formation of SiC at the powder particle surface with increasing temperature. When the same heating experiments were performed at ambient pressure using Argon as flushing gas at 0.3 Nl/min instead

Table 2

Test matrix of the experiments carried out in the laboratory- and hood-furnace with the varying parameters for the investigation of the gas phase reactions. (Heating rate in the Laboratory-furnace was 10 K/min and in the hood furnace 5 K/min).

Device	No	Sample support	Sample[a]	Ar pressure in mbar	Temperature range in °C	Analysis technique
Labor-atory-furnace	1	Graphite sheet, preheated	fine	10	900 … 1400	Image processing
	2	Graphite sheet, preheated	fine	1000	900 … 1400	
	3	BN-coated graphite sheet, preheated	fine	10	1400	
	4	As no 3 + closed crucible	fine	10	900 … 1400	
Hood-furnace	5	Graphite plate, preheated	none	25	400 … 1400	CO-measurement
	6	Graphite plate, not preheated	none	25	400 … 1400	
	7	Graphite plate, preheated	fine	25	400 … 1400	
	8	Graphite plate, not preheated	fine	25	400 … 1400	
	9	Graphite plate, preheated	fine	1000	400 … 1400	
	10	Graphite plate, not preheated	fine	1000	400 … 1400	
	11	Graphite plate, preheated	medium	1000	400 … 1400	
	12	Graphite plate, preheated	coarse	1000	400 … 1400	

'medium' = silicon granulate, size 0.2 … 0.8 mm (Silgrain® HQ from Elkem).

'coarse' = silicon granulate, size 5 … 25 mm (purity of 99.99% from Wacker).

[a] 'Fine' = finely ground silicon powder, size 0 … 10 μm (Silgrain® HQ MicronCut from Elkem).
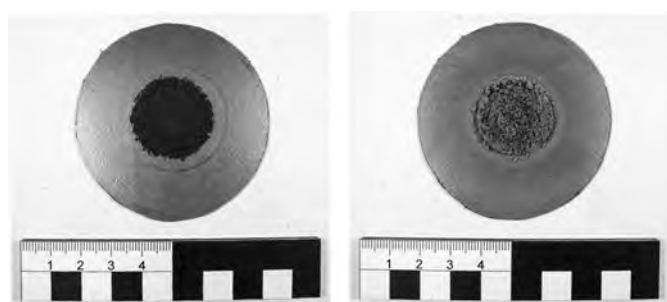
(a) Si powder on uncoated graphite foil before heat treatment.

(b) Same powder after 3 hours holding time at 1375 °C under vacuum.

Fig. 13. Photographic images of the Si powder before and after heating. The brightness change of the silicon powder from black to gray is clearly visible.
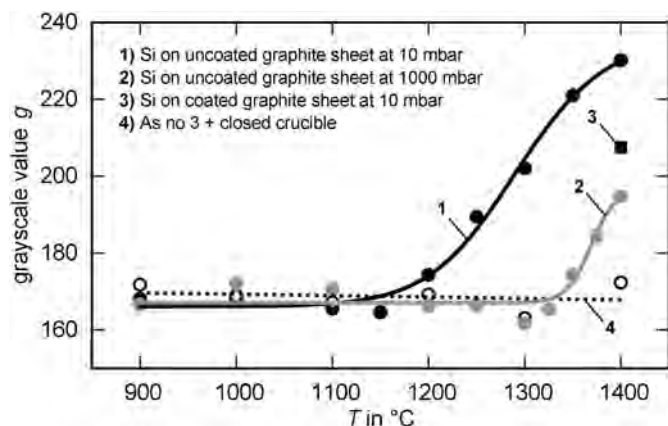
Fig. 14. Grayscale values of Si powder versus heating temperature. – Several configurations of the experimental setup were used to investigate the influence of the carbon source and the pressure.

vacuum, the rise is shifted to about 1350 °C.

When the powder was separated from the furnace by depositing it in a graphite crucible, which was coated with BN and closed by a cover, no SiC formation was detected up to the maximum temperatures used (compare curve 4 in Fig. 14). On the other hand, coating of the graphite sheet with BN and depositing the powder on top of the coating gave only a small reduction of SiC formation compared to the respective experiment without BN coating (compare point 2 in Fig. 14). The latter suggests that C was transported via the gas phase to the silicon powder.

Similar experiments were performed in the larger hood furnace shown in Fig. 6. Differing from the laboratory furnace, this furnace was equipped with a laser photometer for continuous CO measurement as described in section 2. Larger graphite plates (diameter 360 mm) were used as sample support, and a larger amount of Si (58 g) was deposited on top of it – either as powder or as granulate. The graphite plates were either heat treated (5 K/min up to 1500 °C at 25 mbar using an argon flow of 1.3 Nl/min) to remove oxygen impurities before the experiments or used without preheating. After loading with the silicon powder, the same heat treatment was performed: 5 K/min up to 1500 °C at 25 mbar, argon flow 1.3 Nl/min. Results are shown in Fig. 15. The first preheating of the graphite plates significantly reduces CO partial pressure during the second run.

The dominant peak at 1500 °C completely disappears when using preheated graphite plates as a sample support (compare curves 5 and 6 to curves 7 and 8 in Fig. 15). Therefore, this peak is attributed to oxygen adsorbed at the graphite plate. From the comparison of a second heat treatment with and without silicon powder, it can be seen that additional CO is introduced by the silicon powder, which leads to enhanced CO formation at temperatures above 1200 °C. Two CO peaks are identified at temperatures of 1250 °C and 1400 °C, which are attributed to the reduction of SiO_2 powder (compare curves 5 and 7 in Fig. 15).

As with the laboratory furnace, heating cycles were also performed in the hood furnace in argon atmosphere at 1 bar to check for the pressure dependence of the CO reactions. The same fine Si powder as before and – apart from the argon pressure and flow (1 bar and 8 Nl/min) – the same heating conditions were used. Fig. 16 shows the CO partial pressure measured in these experiments. It was significantly
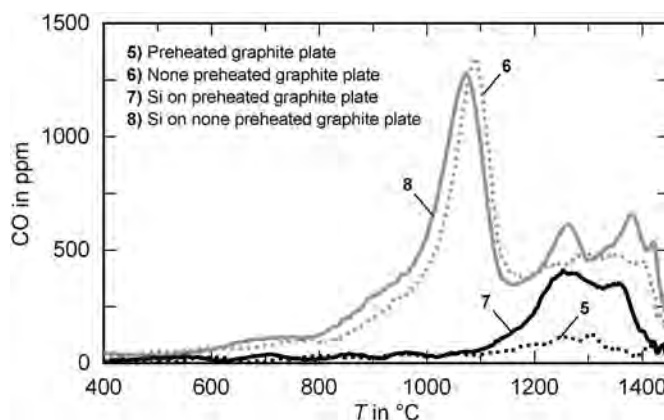
Fig. 15. Comparison of CO measurements of untreated and heat-treated graphite plates, with and without silicon powder at 25 mbar.
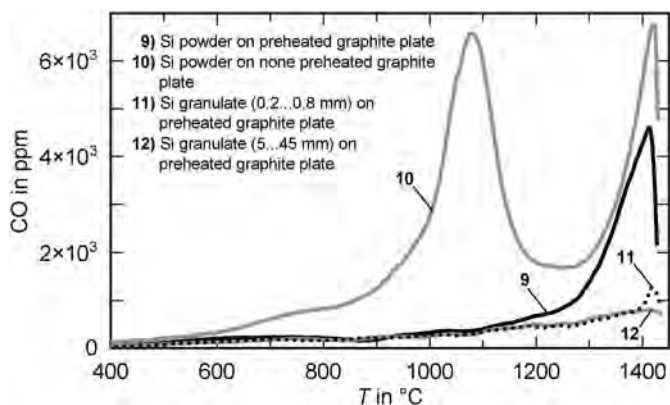
Fig. 16. Comparison of CO measurements of silicon powder on untreated and heat-treated graphite plates in argon atmosphere at normal pressure.

(a) Top view of the slurry coated sample after heat treatment at 1600 °C under vacuum.

(b) SEM image of the coated surface after heat treatment.

Fig. 18. Successful environmental barrier coating by surface infiltration.

higher than in Fig. 15, which is attributed to the CO loss due to continuous evacuation in the 25 mbar experiments. Again, a CO peak is detected at approximately 1400 °C (curve 9). As before, it is attributed to CO formation from the reduction of the oxide layers on the silicon powder. However, the second peak at approximately 1250 °C, which was identified at 25 mbar (compare curve 12 in Fig. 15), has disappeared. The CO peak at 1400 °C becomes significantly smaller, when silicon granules are used instead of the fine powder (compare curve 11 and 12 in Fig. 16). This demonstrates that the specific surface of the powder particles controls the amount of oxygen which is released from the surface layers.

4.2. Investigation of carbon preforms

The results presented in the previous chapters were used to improve the siliconization process of brake disks and EBC coatings which has failed before (compare section 2). For that, the furnaces were baked out before siliconization and only shortly opened during charging. Adsorbed oxygen impurities were removed carefully by repeated flushing and evacuation cycles using highly pure Ar (purity >99.999%).

The infiltration of the brake-disk preform in the TOM_ac furnace was performed at ambient pressure as before, but Ar flow was increased from 0.1 Nl/min to 1 Nl/min. Besides a better removal of CO, this enabled a continuous measurement of CO concentration in the exhaust gas (Fig. 17). In the experiments described in section 2, the CO concentration measured discontinuously at 1000 °C and 1400 °C was 6–8 times higher than in Fig. 17. Using the improved processing conditions, a successful siliconization of the preform was obtained. Note that the two CO peaks attributed to desorption from the preform (Peak I) and to reduction of the SiO_2 layer on the silicon granulate (Peak II) are clearly
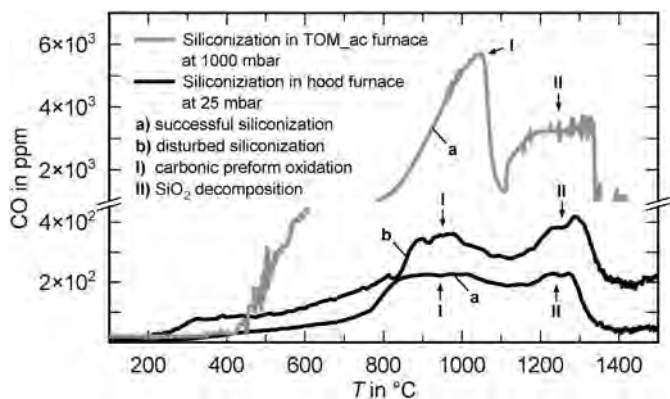

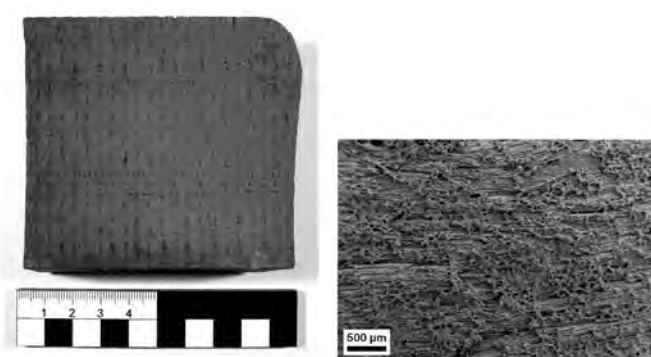**Fig. 17.** Comparison of CO measurements during siliconization in TOM_ac and hood furnace.

visible in this CO measurement.

The infiltration of the carbon preform with the slurry in the hood furnace was successful after carefully baking out the furnace at 1800 °C with repeated flushing and evacuation cycles and using a short charging period. In addition, the sample was dried for 48 h at 130 °C and was installed within a closed graphite crucible coated with boron nitrite. Although the siliconization was performed at a pressure of 25 mbar, CO concentration could be measured continuously with the laser photometer described in section 2. Results are shown in Fig. 17. Again, the two typical CO peaks are detected. The reduction of CO concentration between the failed siliconization (compare Fig. 17) and the successful siliconization (Fig. 18) was less than 50%, but obviously this was sufficient.

5. Discussion of mechanisms and results

The samples shown in Figs. 4 and 11 demonstrate that SiC must have been formed already at lower temperatures prior to the melting of the silicon at 1413 °C [17,18]. In that case, the transfer of the reactants takes place via the gas phase, where SiO and CO are the dominating Si and C species (compare Figs. 11 and 12a. The formation of SiC from SiO and CO is described by the second order reaction:

$$SiO(g) + CO(g) \longrightarrow SiC(s) + O_2(g). \tag{3}$$
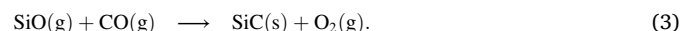
The gas phase transfer of Si leads to a purification – similar to a dry distillation. Therefore, the concentration of Al impurities, which were introduced via the Si granules, is strongly reduced in the SiC formed by reaction 3 compared to SiC formed by melt infiltration. These differences are clearly visible by the XRD and XRF analysis (see Table 1). The greenish color observed in our experiments is typical for high-purity SiC [19,20]. It is concluded that it is a simple indicator for a low quality siliconization.

From the Ellingham diagram (Fig. 19), it can be seen that SiC formation according to Equation (3) is prevented at low temperatures by the larger ΔG of Si oxidation at low temperatures and C oxidation at high temperatures. For all reactions in Fig. 19, a fixed value of the partial pressure of O_2 of [2.6×10^{-16}]bar was used. Note that this affects the slope of all ΔG curves in the same way and does not change the intersections, which are relevant in the discussion below. At a low CO partial pressure of 0.1 mbar, SiC formation from the gas phase should not occur at all because C wins the competition for oxygen (Fig. 19). At a partial pressure of 1 mbar, SiC formation is possible above a temperature of 1280 °C and at 10 mbar above a temperature of 1450 °C (comp. Fig. 19). These temperatures are in agreement with the formation of SiC obtained in experiment 1 and 2 at 1200 °C and 1350 °C (comp. Fig. 14) and also with the growth of SiC whiskers at 1400 °C observed in the TOM_ac furnace (comp. Fig. 3), because CO partial pressure was supposed to increase accordingly in these experiments.
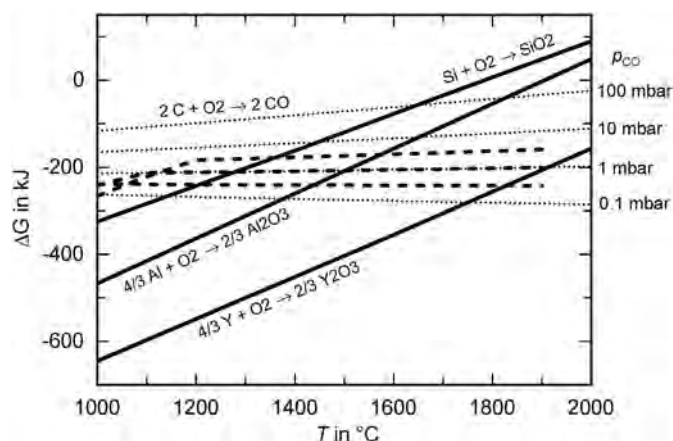
Fig. 19. Ellingham diagram for the reactions of various species with O_2. The reaction $2C + O_2 \rightarrow 2CO$ (dotted lines) is shown for different partial pressures of CO denoted at the scale on the top right of the diagram. The three dashed lines represent the reaction $SiC + O_2 \rightarrow SiO + CO$, calculated for the equilibrium SiO partial pressures shown in Fig. 12 a; the upper dashed line is calculated for a CO partial pressure of 10 mbar, the medium dashed line for 1 mbar and the lower dashed line for 0.1 mbar.

For the reduction of SiO_2 observed in the in-situ experiments (comp. Figs. 15–17), carbon has to be transferred via the gas phase to the sample. This is explained by the non-equilibrium conditions existing in the graphite furnaces used. We assume that within the graphite felt and close to the graphite heaters of the furnaces the thermodynamic equilibrium shown in Fig. 11 is almost achieved. On the other hand, within the silicon powder carbon activity initially is low. This means that some carbon can be deposited according to Equation (2) by dissociation of CO until carbon activity is unity. CO_2, which is formed by reaction 1 is removed by the gas stream, and carbon may react with the sample (see below). Both effects lead to additional carbon deposition by dissociation of CO. In addition, during the heating stage more carbon can be deposited, because the sample is cooler than the heaters and the outer layers of the graphite felt of the furnace. This means that the equilibrium CO_2/CO-ratio at the sample is higher than that of the furnace and CO dissociation is favorable. Carbon reduces SiO_2 at high temperature and low CO partial pressure. The free energy of the respective reactions is illustrated in the Ellingham diagram (comp. Fig. 19). The temperature at the intersection of the ΔG lines, where reduction by carbon becomes favorable, decreases with CO partial pressure. E. g., SiO_2 is reduced above 1280 °C at a CO partial pressure of 1 mbar and above 1150 °C at 0.1 mbar. Note, that below these temperatures Si is oxidized by CO. The temperatures for SiO_2 reduction nicely fit to the temperatures between 1150 °C and 1400 °C of the second CO peak during the in-situ experiments (comp. Figs. 15–17).

The experiments 1 and 2 show a shift of visible SiC formation on the Si particles from about 1200 °C to 1350 °C, when total pressure is increased from 10 mbar to 1 bar (compare Fig. 14). These temperatures are significantly higher than the temperatures expected from thermodynamic calculation (compare Fig. 12). It is concluded that SiC formation is hindered by an oxide scale at the surface of the SiO_2 particles. Only after the oxide scale is removed by reduction of SiO_2, significant SiC formation can take place. The reduction of SiO_2 by CO can start at 1140 °C at a CO partial pressure of 0.1 mbar and is shifted to higher temperatures when CO partial pressure increases (comp. Fig. 19). This perfectly fits to the peaks observed in the in-situ experiments (comp. Figs. 15–17). Tracer diffusion experiments with ^{18}O and ^{13}C showed that CO can diffuse within the SiO_2 layer at temperatures of 1100 °C [21]. Above 1180 °C, CO reacts with Si and forms SiC at the Si/SiO_2 interface [22,23]. Yet, it is assumed that the reduction of the SiO_2 layer observed in the present study drastically increases the rate of SiC formation. Obviously, the increase of total pressure in the laboratory furnace is

associated with an increase of CO partial pressure, as it was measured in the hood furnace (comp. Figs. 15 and 16). The CO measurements in the hood furnace demonstrate that at low pressure and corresponding low CO partial pressure the onset of SiO_2 reduction shifts to lower temperatures. It is spread over a larger temperature range which may be caused by the retarding effect of increasing CO partial pressure predicted by the thermodynamic calculation. For a successful infiltration of Si, the balance between silicon oxide formation and reduction should be slightly on the oxide side, preventing SiC formation. However, this is a delicate balance, and it was shown that a small reduction of CO partial pressure from 0.4 mbar to 0.2 mbar decides upon a successful infiltration (compare Fig. 17).

The formation of oxide scales on Si has been intensively investigated, because it is widely used in semiconductor processing [24,25] and the interaction of CO with SiO_2 scales on Si and SiC has been explored as it is relevant for the carbothermic reduction processes, which can be relevant for Si production [26] and wafer growth [21]. Depending on the gas flow, the furnace atmosphere (O_2 and H_2O content) and the time-temperature cycle, SiO_2 layers between 1 … 50 nm thickness are likely to form, where existing H_2O significantly accelerates the layer growth [24,25]. In situ ellipsometry was used to study the growth of SiO_2 layers on Si and SiC substrates in the temperature range between 890 °C and 1220 °C [27]. Slightly thicker layers up to 200 nm were observed [22,23]. As the temperature rises further, a carbothermal reduction of the SiO_2 layer to CO and SiO takes place. Due to the reduction of the layer thickness and the formation of CO, the SiC layer grows increasingly faster, until the SiO_2 layer has been completely reduced and – if the Si is still in excess – a SiC shell is left around the residual silicon. The SiO again forms SiC on the carbon substrate, where the released oxygen oxidizes further carbon to CO and thus maintains the SiC formation as a catalyst [13,28].

The formation of an oxide layer on the silicon powder and its conversion to SiC at temperatures above 1100 °C, as it is observed in the present paper, is consistent to these results. A similar decrease of the temperature for SiO_2 reduction with decreasing gas pressure was already reported in a thermodynamic study of Loutzenhiser et al. [26]. However, restrictions in the transfer of the equilibrium calculations to the real process should be taken into account as discussed in the previous section. Very large discrepancies are expected especially at high vacuum conditions, because the very low partial pressures of the gaseous reaction products used in the thermodynamic equations are not realistic in the vicinity of the charge.

Similar gas phase reaction, as reported here for SiO_2, are also relevant for heat treatments with other oxides in graphite furnaces. Thus, a novel carbothermic reduction of alumina was proposed based on thermodynamic calculations within the EU project ENEXAL [29]. A significant decrease of reduction temperature was predicted, when pressure was reduced from ambient to 0.1 bar. A similar decrease of intersection temperatures for the ΔG lines of C and Al is shown in Fig. 19, when CO partial pressure is decreased from 100 mbar to 0.1 mbar. Another important application of graphite furnaces is liquid phase sintering of non-oxide ceramics such as SiC, Si_3N_4 or AlN. The liquid phase is formed from eutectic mixtures of oxide additives, e. g.: SiO_2, Al_2O_3 or rare earth oxides. The Ellingham diagram for the reaction of Si, Al, Y and C with O_2 enables a direct comparison of the stability of the respective oxides (comp. Fig. 19). It is concluded that yttria is most stable against reduction and alumina is slightly more stable than silica. Selective reduction of oxides during the sintering process leads to a change of their composition and an increase of the temperature of liquid phase formation. CO_2 which is formed during the reduction forms CO according to reaction 1, when it comes into contact with hot graphite parts of the furnace. By this, a CO cycle is established and liquid phase sintering is continuously shifted to higher temperatures or even prevented completely. It was demonstrated experimentally by the group of one of the authors that very small CO concentrations below 1000 ppm can already cause serious problems in sintering of AlN [30]. In the eutectic

mixture of Al_2O_3 and Y_2O_3, the Al_2O_3 was preferentially reduced and melting shifted to higher temperatures. An indicator for the CO effect on sintering of non-oxide ceramics is an inhomogeneous discoloration of those parts, which are exposed more directly to furnace atmosphere [30].

On the other hand, a complementary experiment was done by Ihle et al., where CO was added directly to the Ar flushing gas during sintering of SiC – Al_2O_3 mixtures. At the high CO partial pressure used in these experiments, Al_2O_3 reduction could be prevented. Without CO addition, Al_2O_3 was reduced to Al [31]. It is confirmed by Fig. 19 that Al_2O_3 is stable at a CO partial pressure of 100 mbar up to 1830 °C. Thus, depending on partial pressure CO can either have a reducing or an oxidizing effect in graphite furnaces.

6. Conclusions

Using different graphite heated furnaces, the negative effects of O_2 on the siliconization process have been demonstrated. Various heating experiments, microstructure and thermodynamic analyses were used to identify the underlying mechanisms. The proposed mechanisms are consistent to investigations already published for other high temperature processes. CO formed from O_2 impurities within graphite furnaces can have oxidizing, reducing or carburizing effects depending on partial pressure and environment. But it affects many heat treatments and is a cause for inadmissible process variations. From the results above, the following measures are deduced to reduce or even prevent a disturbing influence of oxygen on the liquid silicon infiltration process.

(i) Drying and heat treatment of the preforms before siliconization to remove humidity and promote outgassing.
(ii) Avoiding contact between carbon and silicon by coating corresponding carbon parts (e. g. coating graphite crucibles with boron nitride) and shielding the charge from gaseous carbon sources (e. g. using closed crucibles or CO getter).
(iii) Use of silicon granules as coarse as possible to reduce its specific surface and thereby the amount of oxygen introduced by the granulate. This also reduces the ratio of SiC (from the shell eventually formed around the silicon grain) to Si, so that in the best case SiC can be completely dissolved in the Si melt.

There are additional measures which should be used in graphite furnaces for all processes which are sensitive to oxygen impurities.

(iv) Using graphite felt with a high degree of graphitization and corresponding low water absorption.
(v) Carefully checking for vacuum leakages at the furnace and the gas supply system.
(vi) Removal of oxygen introduced by absorption in the insulation and the kiln furniture by backing the furnace above the maximum temperature of the subsequent thermal process, and subsequent flushing-evacuation-cycles with inert gas.
(vii) Avoiding long periods for opening and charging the furnace.
(viii) Using a preferably large flow of highly pure inert gas to flush away oxygen containing gas species.

Even if all these precautions are considered, the authors' practical experience show that siliconization and sintering processes in graphite furnaces sometimes fail. This is attributed to leakages which occur on sealings especially due to charging of the furnaces. Fatigue and crack formation in the steal enclosure due to thermal cycling may also occur. Moreover, inert gas quality may be lower than expected. Altogether, this makes clear that a continuous monitoring of CO concentration is essential to guarantee a reproducible quality of heating processes in graphite furnaces. For this purpose, two options have been presented in the present paper (compare section 2).

1. An electrochemical CO sensor (e. g., a combustion gas analyzer) can be installed in the exhaust gas flow.
2. A laser photometer consisting of a laser diode and a photo diode can be mounted in the cold part of the furnace.

Whereas option 1 can be realized very simply, more care has to be taken to install the laser photometer. On the other hand, the photometer also provides CO data without gas flow, e. g., when operating in a vacuum. In either case, absolute values of CO concentration at the position of the charge are difficult to obtain. But for the routine operation of the furnaces, only the trends in the CO signals are relevant. The control and warning limits required for process control can be derived empirically from a correlation of CO data with product quality.

Declaration of competing interest

The authors declare that they have no known competing financial interests or personal relationships that could have appeared to influence the work reported in this paper.

Acknowledgements

References

[1] P.J. Hofbauer, E. Rädlein, F. Raether, Fundamental mechanisms with reactive infiltration of silicon melt into carbon capillaries, Adv. Eng. Mater. 21 (8) (2019) 1–11.
[2] P.J. Hofbauer, F. Raether, E. Rädlein, Finite element modeling of reactive liquid silicon infiltration, J. Eur. Ceram. Soc. 40 (2) (2020) 251–258.
[3] A. Kienzle, H. Jäger, Carbon-fiber-reinforced Silicon Carbide: a New Brake Disk Material, 2015.
[4] M.R. Krödel, P.J. Hofbauer, G. Luichtel, J. Katzer, M. Tausendfreund, G. Derst, Production of Mirrors Made of Hb-Cesic® for an Airborne Reconnaissance Telescope System, 2009.
[5] P.J. Hofbauer, M.R. Krödel, Designing Optimized, Ultra-lightweighted Mirror Structures Made of Cesic® for Space and Ground Based Applications, 2010.
[6] F. Raether, J. Meinhardt, A. Kienzle, Oxidation behaviour of carbon short fibre reinforced c/sic composites, J. Eur. Ceram. Soc. 27 (2–3) (2007) 1217–1221.
[7] S. Beyer, S. Schmidt-Wimmer, K. Quering, C. Wilhelmi, M. Steinhilber, Technology Status of Fuel Cooled Ceramic Matrix Composites for Dual-Mode Ramjet (Dmr) and Liquid Rocket Engine (Lre) Applications, 2012.
[8] F.H. Gern, R. Kochendörfer, Liquid silicon infiltration: description of infiltration dynamics and silicon carbide formation, Compos. Appl. Sci. Manuf. 28 (4) (1997) 10.
[9] F. Raether, R. Hofmann, G. Müller, H.J. Sölter, A novel thermo-optical measuring system for the in situ study of sintering processes, J. Therm. Anal. Calorimetry 53 (3) (1998) 717–735.
[10] F. Raether, R. Springer, S. Beyer, Optical dilatometry for the control of microstructure development during sintering, Mater. Res. Innovat. 4 (4) (2001) 245–250.
[11] N.P. Bansal, J. Lamon, Ceramic Matrix Composites: Materials, Modeling and Technology, John Wiley & Sons, Inc., Hoboken, New Jersey, 2015.
[12] H.F. Andersen, C.E.L. Foss, J. Voje, R. Tronstad, T. Mokkelbost, P.E. Vullum, A. Ulvestad, M. Kirkengen, J.P. Mæhlen, Silicon-carbon composite anodes from industrial battery grade silicon, Sci. Rep. 9 (14814) (2019) 1–9.
[13] M. Saito, S. Nagashima, A. Kato, Crystal growth of sic whisker from the sio(g)-co system, J. Mater. Sci. Lett. 11 (7) (1992) 373–376.
[14] K. Cheong, Z. Lockman, Effects of temperature and crucible height on the synthesis of 6h-sic nanowires and nanoneedles, J. Alloys Compd. 481 (2009) 345–348.
[15] M. Nagamori, I. Malinsky, A. Claveau, Thermodynamics of the si-c-o system for the production of silicon carbide and metallic silicon, Metall. Trans. A B 17 (1986) 503–514.
[16] S. Group, Sigraflex® asbestfreier dichtungswerkstoff aus flexilbem naturgraphit, 2009.
[17] W.F. Knippenberg, G. Verspui, The influence of impurities on the growth of silicon carbide crystals grown by gas-phase reactions, Mater. Res. Bull. 4 (1969) 33–44.
[18] P.J. Hofbauer, In-situ-Messung und Simulation der Flüssigphasensilicierung, 21, Universitätsverlag Ilmenau, Ilmenau, 2020 of Werkstofftechnik Aktuell.
[19] H. Fuchs, Siliciumcarbid, Chemie Ingenieur Technik 46 (4) (1974) 139–142.
[20] K. Zekentes, K. Rogdakis, Sic nanowires: material and devices, J. Phys. Appl. Phys. 44 (133001) (2010) 1–17.

[21] C.D. Cavellin, I. Trimaille, J.-J. Ganem, M. D'Angelo, I. Vickridge, A. Pongracz, G. Battistig, An [18]o study of the interaction between carbon monoxide and dry thermal sio_2 at 1100°c, J. Appl. Phys. 105 (2009) 1–7, 033501.

[22] O.H. Krafcsik, G. Vida, I. Pócsik, K.V. Josepovits, P. Deák, Carbon diffusion through sio_2 from a hydrogenated amorphous carbon layer and accumulation at the sio_2/si interface, Jpn. J. Appl. Phys. 40 (4A) (2001) 2197–2200.

[23] O.H. Krafcsik, G. Vida, K.V. Josepovits, P. Deák, G.Z. Radnóczi, B. Pécz, I. Bársony, Void-free epitaxial growth of cubic sic crystallites during co heat treatment of oxidized silicon, Mater. Sci. Forum 389–393 (2002) 359–362.

[24] M. Naito, H. Homma, N. Momma, A practical model for growth kinetics of thermal sio_2 on silicon applicable to a wide range of oxide thickness, Solid State Electron. 29 (9) (1986) 885–891.

[25] D. Lafatzis, K. Mergia, Oxidation behaviour of si wafer substrates in air, J. Appl. Phys. 114 (144308) (2013) 1–9.

[26] P.G. Loutzenhiser, O. Tuerk, A. Steinfeld, Production of si by vacuum carbothermal reduction of sio_2 using concentrated solar energy, J. Mineralstoffwechsel: Alternative Energy Mater. Process. 62 (9) (2010) 49–54.

[27] Y. Hijikata, S. Yagi, H. Yaguchi, S. Yoshida, Thermal Oxidation Mechanism of Silicon Carbide, InTech, Rijeka, 2013, pp. 181–206, 7.

[28] Y. Endo, Y. Yatsurugi, Y. Terai, T. Nozaki, Equilibrium of carbon and oxygen in silicon with carbon monoxide in ambient atmosphere, J. Electrochem. Soc. 126 (8) (1979) 1422–1425.

[29] E. Balomenos, D. Panias, I. Paspaliaris, A. Steinfeld, E. Guglielmini, B. Friedrich, B. Jaroni, M. Halmann, M. Epstein, I. Vishnevsky, Carbothermic reduction of alumina: a review of developed processes and novel concepts, in: European Metallurgical Conference, Vol. 1, GDMB e.V., pp. 729–744.

[30] A. Klimera, Festigkeitssteigerung von aluminiumnitrid-keramiken, Dissertation, bayerischen Julius-Maximilians-Universität Würzburg, 2008.

[31] J. Ihle, M. Herrmann, J. Adler, Phase formation in porous liquid phase sintered silicon carbide: Part i: interaction between al_2o_3 and sic, J. Eur. Ceram. Soc. 25 (7) (2005) 987–995.